

# Optical facet coatings for high-performance LWIR quantum cascade lasers at $\lambda \sim 8.5 \mu\text{m}$

MA Yuan<sup>1,2</sup>, LIN Yu-Zhe<sup>1\*</sup>, WAN Chen-Yang<sup>1,2</sup>, WANG Zi-Xian<sup>1,2</sup>, ZHOU Xu-Yan<sup>1,3</sup>, ZHANG Jin-Chuan<sup>4</sup>, LIU Feng-Qi<sup>4</sup>, ZHENG Wan-Hua<sup>1,2\*</sup>

- (1. Laboratory of Solid-State Optoelectronics Information Technology, Institute of Semiconductors, Chinese Academy of Sciences, Beijing 100083, China;
2. Center of Materials Science and Optoelectronics Engineering, University of Chinese Academy of Sciences, Beijing 100049, China;
3. Weifang Academy of Advanced Opto-Electronic Circuits, Weifang 261021, China;
4. Key Laboratory of Semiconductor Materials Science, Institute of Semiconductors, Chinese Academy of Sciences, Beijing 100083, China)

**Abstract:** We report on the performance improvement of long-wave infrared quantum cascade lasers (LWIR QCLs) by studying and optimizing the anti-reflection (AR) optical facet coating. Compared to  $\text{Al}_2\text{O}_3$  AR coating, the  $\text{Y}_2\text{O}_3$  AR coating exhibits higher catastrophic optical mirror damage (COMD) level, and the optical facet coatings of both material systems have no beam steering effect. A 3-mm-long cavity length, 9.5- $\mu\text{m}$ -wide buried heterostructure (BH) LWIR QCL of  $\lambda \sim 8.5 \mu\text{m}$  with  $\text{Y}_2\text{O}_3$  metallic high-reflection (HR) and AR of  $\sim 0.2\%$  reflectivity coating demonstrates a maximum pulsed peak power of 2.19 W at 298 K, which is 149% higher than that of uncoated device. For continuous-wave (CW) operation, by optimizing the reflectivity of the  $\text{Y}_2\text{O}_3$  AR coating, the maximum output power reaches 0.73 W, which is 91% higher than the uncoated device.

**Key words:** quantum cascade lasers, long-wave infrared, optical facet coatings

**PACS:**

## 8.5 $\mu\text{m}$ 高性能长波红外量子级联激光器的光学腔面镀膜研究

马 源<sup>1,2</sup>, 林羽喆<sup>1\*</sup>, 万晨杨<sup>1,2</sup>, 王紫纤<sup>1,2</sup>, 周旭彦<sup>1,3</sup>, 张锦川<sup>4</sup>, 刘峰奇<sup>4</sup>, 郑婉华<sup>1,2\*</sup>

- (1. 中国科学院半导体研究所 固态光电信息技术重点实验室, 北京 100083;
2. 中国科学院大学 材料科学与光电工程中心, 北京 100049;
3. 潍坊先进光电芯片研究院, 山东 潍坊 261021;
4. 中国科学院半导体研究所 半导体材料科学重点实验室, 北京 100083)

**摘要:** 我们通过研究和优化长波红外量子级联激光器(LWIR QCLs)的光学腔面增透(AR)膜来提高器件的输出性能。与 $\text{Al}_2\text{O}_3$ 膜系相比, $\text{Y}_2\text{O}_3$  AR膜表现出更高的灾难性光学镜损伤(COMD)水平,两种膜系的光学腔面镀膜均无光束转向效应。对激励波长为8.5  $\mu\text{m}$ 的3 mm腔长、9.5  $\mu\text{m}$ 脊宽掩埋异质结(BH)LWIR QCL使用 $\text{Y}_2\text{O}_3$ 膜系的金属高反(HR)膜和反射率约0.2%的AR膜,在298 K下获得了2.19 W的最高脉冲峰值功率,较未镀膜器件提高149%。对于连续(CW)操作,通过优化 $\text{Y}_2\text{O}_3$  AR膜的反射率,最高输出功率达到0.73 W,较未镀膜器件提高91%。

**关键词:** 量子级联激光器;长波红外;光学腔面镀膜

中图分类号: O43; TN248.4 文献标识码: A

Received date: 2023- 11- XX,

收稿日期: 2023- 11-

Foundation items: Supported by the National Natural Science Foundation of China (Grant No. 12393830).

Biography: MA Yuan (1997-), male, Xincui, Henan, Ph. D. Research area involves semiconductor materials and devices. E-mail: mayuan@semi. ac. cn.

\* Corresponding author: E-mail: linyuzhe@semi. ac. cn, whzheng@semi. ac. cn

## Introduction

As a significant candidate for highly efficient and compact mid-infrared (MIR) to terahertz light sources, quantum cascade lasers (QCLs) have shown tremendous potential in applications such as chemical and biological sensing<sup>[1, 2]</sup>, free space optical communication<sup>[3]</sup>, and infrared countermeasures (IRCM)<sup>[4]</sup>. Among them, more and more attentions have been devoted to the development of long-wave infrared (LWIR,  $\lambda \approx 8\text{-}12\ \mu\text{m}$ ) QCLs with high output power, high wall-plug efficiency (WPE) and good beam quality<sup>[5-7]</sup>. However, some problems still need to be solved, which brings greater challenges to the performance improvement of LWIR QCLs. First, additional waveguide designs or thicker epitaxial structures need to be considered in order to maintain optical confinement factor of LWIR QCLs<sup>[8]</sup>. Otherwise, the reduction in mode gain, the increase in free carrier absorption losses (proportional to  $\lambda^2$ ) and the enhancement of plasmonic mode coupling at the metal-semiconductor interface will significantly deteriorate device performance<sup>[9]</sup>. Second, optical facet coating, as a key technology, has important applications in power extraction<sup>[10]</sup>, self-lasing suppression of single-mode lasers<sup>[11]</sup>, etc. Nevertheless, cavity facet coating of LWIR QCLs requires not only increasing thickness of anti-reflection (AR) coating to match the target wavelength<sup>[12]</sup>, but also select an appropriate coating material to reduce facet optical absorption, thereby improving the level of catastrophic optical mirror damage (COMD)<sup>[13]</sup>. Additionally, it is necessary to avoid deterioration of beam quality due to beam steering effect<sup>[14]</sup>. Metallic high-reflection (HR) coatings have been commonly used and studied in LWIR QCLs to improve one facet output power<sup>[15-17]</sup>. Currently, there are relatively few reports on the optimization of AR coatings.

In this letter, two types of optical facet coatings ( $\text{Al}_2\text{O}_3$  and  $\text{Y}_2\text{O}_3$ ) were demonstrated and compared on  $8.5\ \mu\text{m}$  LWIR QCLs for the selection of appropriate coating material. By optimizing a single-layer  $\text{Y}_2\text{O}_3$  AR coating on the 3-mm-long cavity length buried heterostructure (BH) ridge LWIR QCLs, the continuous-wave (CW) and pulsed performance had been significantly improved. Corresponding deterioration of far-field characteristics after coating was not observed.

## 1 Wafer structure, Fabrication and testing

The LWIR QCL wafer, lasing wavelength close to  $8.5\ \mu\text{m}$ , is based on a single phonon resonance-continuum depopulation structure with 35 cascade stages. The active region consists of lattice-matched  $\text{In}_{0.53}\text{Ga}_{0.47}\text{As}/\text{In}_{0.52}\text{Al}_{0.48}\text{As}$  layers as previously shown in Ref. [18]. The double channel ridge structure with an average ridge width of  $9.5\ \mu\text{m}$  was first fabricated by contact photolithography and wet chemical etching. Then, semi-insulating  $\text{InP}:\text{Fe}$  is grown by MOCVD in order to confine the carriers and reduce sidewall optical losses. A 400-nm-

thick  $\text{SiO}_2$  layer was deposited by Plasma Enhanced Chemical Vapor Deposition (PECVD) for insulation, and a Ti/Au top contact layer was deposited by e-beam evaporation for electrical contacts. An additional  $5\text{-}\mu\text{m}$ -thick gold layer was subsequently electroplated to further improve heat dissipation. After thinned to  $120\ \mu\text{m}$ , an AuGeNi/Au bottom contact layer was deposited on the substrate. The processed QCL wafer was cleaved into bars with a cavity length of 3 mm for facet coating.

The uncoated and coated devices were mounted episcide down on diamond submounts with indium for higher heat dissipation efficiency. The CW and pulsed (5 kHz,  $1\ \mu\text{s}$ ) performance were characterized by a Thorlabs S450C calibrated thermopile power meter and IS50R Fourier Transform Infrared (FTIR) spectrometer. We used the rotation method to test the far-field divergence angle and built an automated scanning system.

## 2 Coating material processing and comparison

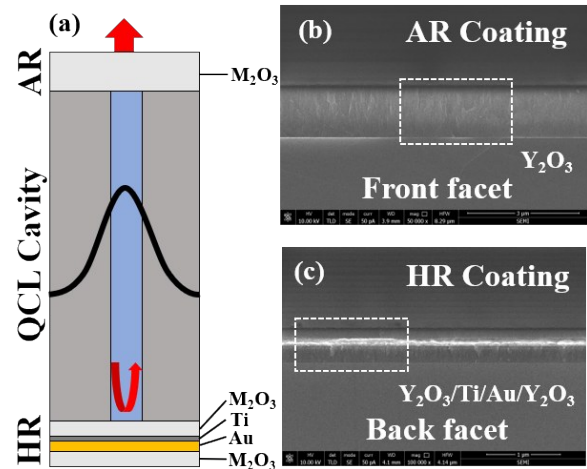


Fig. 1 (a) Schematic diagram of the LWIR QCLs with AR and HR coatings applied to the front and back facets, scanning electron microscopy (SEM) images of coatings on (b) front and (c) back facet

图1 (a) LWIR QCLs 前、后腔面 AR 和 HR 膜的示意图, (b) 前和 (c) 后腔面膜的扫描电镜图

Dielectric material used as LWIR QCLs facet coating must have low absorption in the LWIR range and mature fabrication process to ensure that the AR coating does not suffer from COMD. For this purpose,  $\text{Al}_2\text{O}_3$  and  $\text{Y}_2\text{O}_3$  facet coating material systems were studied from the same wafer with 3 mm cavity length. The metallic HR coating consisting of  $\text{M}_2\text{O}_3/\text{Ti}/\text{Au}/\text{M}_2\text{O}_3$  was coated on the back facet, as shown in Figure 1(a). The AR coating was the single-layer of  $\text{M}_2\text{O}_3$  coated on the front facet, where  $\text{M}_2\text{O}_3$  represents  $\text{Al}_2\text{O}_3$  or  $\text{Y}_2\text{O}_3$ . A dielectric material  $\text{M}_2\text{O}_3$  was deposited on the back facet using e-beam evaporation to provide electrical insulation from the Au. After that, a thin layer of Ti was sputtered to increase the adhesion between  $\text{M}_2\text{O}_3$  and Au. Next, 100 nm of Au with a high refractive index was used to achieve a high reflection of nearly 100 % for the LWIR QCLs. Finally,

another layer of dielectric material  $\text{M}_2\text{O}_3$  was deposited to complete the HR coating to avoid short-circuiting of the devices in the subsequent packaging process. E-beam evaporation was chosen to deposit a single-layer of  $\text{M}_2\text{O}_3$  AR coating. The AR reflectivity between 27 % (uncoated) and close to 0 % (quarter-wave layer) can be adjusted by simply adjusting the coating thickness<sup>[10]</sup>. The AR and HR scanning electron microscope (SEM) image of  $\text{Y}_2\text{O}_3$  material system as shown in Figure 1(b) and (c).

Simulation based on characteristic transfer matrix was derived to determine the coating thickness at the corresponding reflectivity. Reflectance measurements were performed on a FTIR spectrometer with an MCT detector. Figure 2 shows the optical curves of the simulations and measurements of the  $\text{Al}_2\text{O}_3$  and  $\text{Y}_2\text{O}_3$  AR coatings. The wavelength for an uncoated LWIR QCL is shown in the inset. The theoretical simulations are in good agreement with the experimental measurements.

For  $\text{Al}_2\text{O}_3$  material system, the thickness at quarter-wave layer exceeds  $2 \mu\text{m}$ , which poses great difficulties in manufacturing. Therefore, in the initial stage, we selected a single-layer  $\text{Al}_2\text{O}_3$  AR coating with a reflectivity of  $\sim 8.0 \%$  by reducing the thickness, and the HR coating was  $\text{Al}_2\text{O}_3/\text{Ti}/\text{Au}/\text{Al}_2\text{O}_3$ . The CW light-current-voltage ( $L$ - $I$ - $V$ ) and WPE curves of uncoated and HR-AR ( $R \approx$

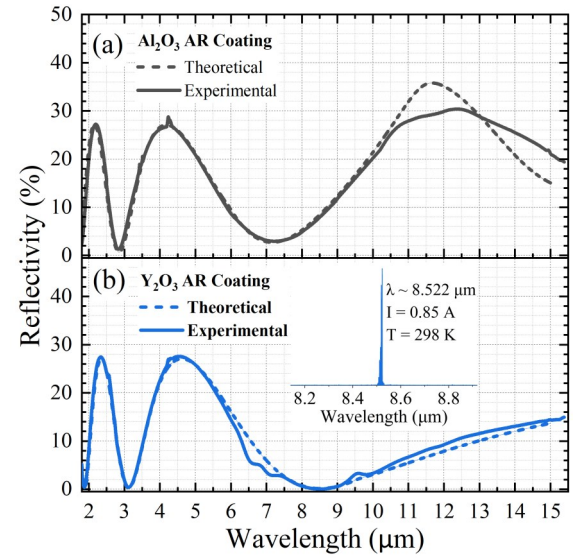


Fig. 2 Experimental and theoretically simulated reflectance curves of (a)  $\text{Al}_2\text{O}_3$  and (b)  $\text{Y}_2\text{O}_3$  AR coatings. The inset shows the lasing spectrum of the LWIR QCL at 298 K  
图2 (a)  $\text{Al}_2\text{O}_3$ 和(b)  $\text{Y}_2\text{O}_3$  AR膜的实验和理论模拟反射率曲线,插图是LWIR QCL在298 K的激光光谱

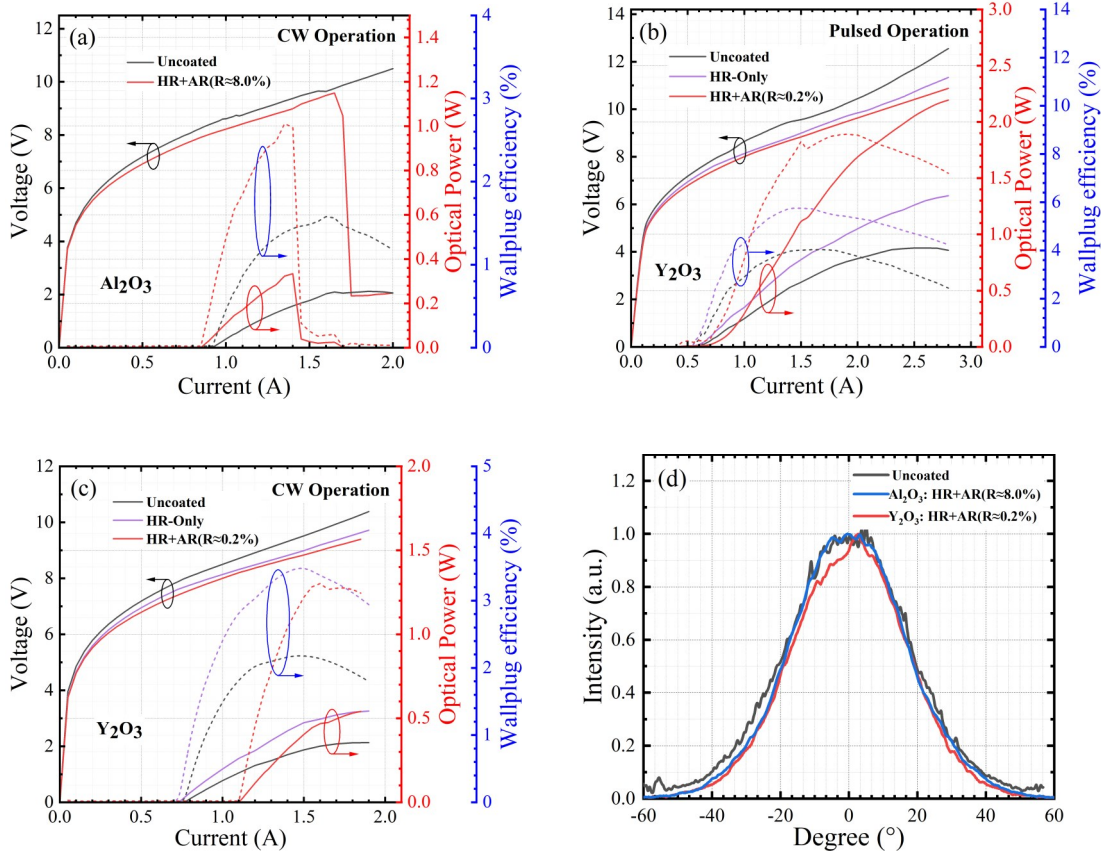


Fig. 3  $L$ - $I$ - $V$  and WPE curves of the QCLs at 298 K, (a) CW operation of uncoated and HR-AR ( $\text{Al}_2\text{O}_3$  coating), (b) pulsed and (c) CW operation of uncoated, HR-only and HR-AR ( $\text{Y}_2\text{O}_3$  coating). (d) Measured lateral far-field profiles

图3 QCL在298 K时的 $L$ - $I$ - $V$ 和WPE曲线,(a)连续操作的未镀膜、AR-HR( $\text{Al}_2\text{O}_3$ 膜系)器件,(b)脉冲和(c)连续操作的未镀膜、仅HR和AR-HR( $\text{Y}_2\text{O}_3$ 膜系)器件,(d)测量的水平远场分布



8 %) coated devices operating at 298 K are shown in Figure 3(a). Among them, the solid lines in the black and red circles represent the voltage and optical power curves, respectively, while the dashed lines in the blue circle represent the WPE curve. Compared with uncoated and coated devices, the slope efficiency ( $\eta_s$ ) has been improved from 0.42 to 0.7 W/A, while WPE has been increased from 1.6 to 2.7 %. Moreover, the maximum output power ( $P_{max}$ ) increased from 0.25 to 0.33 W. However, the coated devices using  $\text{Al}_2\text{O}_3$  exhibit COMD at the power density level of  $\sim 1.73 \text{ MW/cm}^2$  before thermal inversion, as shown in Figure 4(a). This also shows that  $\text{Al}_2\text{O}_3$  coating has high absorption in the LWIR range<sup>[19]</sup>, with an absorption coefficient as high as  $755.2 \text{ cm}^{-1}$  at  $8.5 \mu\text{m}$ , which is not suitable for power extraction of high-performance LWIR QCLs.

In comparison,  $\text{Y}_2\text{O}_3$  material system exhibits better performance. Since  $\text{Y}_2\text{O}_3$  has a higher refractive index in the LWIR range, the thickness of the AR coating is initially set to quarter-wave layer with reflectivity of  $\sim 0.2 \%$ . The pulsed  $L$ - $I$ - $V$  and WPE curves of uncoated, HR-only and HR-AR coated devices operating at 298 K are shown in Figure 3(b).  $\eta_s$  from 0.65 W/A for uncoated, 0.88 W/A for HR-only, to a higher value of 1.63 W/A for HR-AR device. WPE from 4.0, 5.8 to 8.8 % and  $P_{max}$  from 0.88, 1.34 to 2.19 W. The HR-AR coated device shows 120 % and 149 % improvements in WPE and  $P_{max}$ , respectively compared to uncoated device under 298 K in pulsed mode. Since the absorption coefficient of  $\text{Y}_2\text{O}_3$  at  $8.5 \mu\text{m}$  is only  $8.3 \text{ cm}^{-1}$ <sup>[20, 21]</sup>. Its cavity surface remained normal after the test, as shown in Figure 4(b). The COMD has not occurred until the power density reaching  $11.5 \text{ MW/cm}^2$ . The  $L$ - $I$ - $V$  and WPE curves of these devices under 298 K CW operation are shown in Figure 3(c), representing an improvement of  $\eta_s$  from 0.50 W/A for uncoated, 0.68 W/A for HR-only, to 1.07 W/A for HR-AR laser, WPE from 2.2, 3.5 to 3.3 % and  $P_{max}$  from 0.35, 0.54 to 0.54 W.

Under CW operation, the WPE and  $P_{max}$  of HR-AR coated device increased by 50 % and 54 % respectively compared to uncoated device. However, it showed no significant improvement compared to only HR device. The threshold current density  $J_{th}$  of LWIR QCLs is defined as<sup>[22]</sup>

$$J_{th} = J_{tr} + \frac{\alpha_w + \alpha_m}{g\Gamma}, \quad (1)$$

where  $J_{tr}$  is the transparency current,  $\alpha_w$  is the internal loss of the laser waveguide,  $\alpha_m = (1/2L)\ln[1/R_{front}R_{back}]$  is the overall mirror loss,  $L$  is the length of the cavity, and  $g\Gamma$  is the differential modal gain.  $\alpha_m$  increases significantly from  $2.2 \text{ cm}^{-1}$  for the only-HR device to  $10.4 \text{ cm}^{-1}$  for the HR-AR ( $R \approx 0.2 \%$ ) device. According to Eq. (1), the  $J_{th}$  of CW operation significantly increase from  $2.50 \text{ kA/cm}^2$  to  $3.82 \text{ kA/cm}^2$ . This substantial increase in threshold current density brings additional self-heating effects to the devices<sup>[15]</sup>, which appears to impede AR coating from further extracting power.

One concern with optical coatings is the beam steering effect<sup>[12, 14]</sup>. Conversely, the lateral far-field divergence angle of the HR+AR devices with  $\text{Al}_2\text{O}_3$  and  $\text{Y}_2\text{O}_3$  coatings shown in Figure 3(d) is consistent with that of the uncoated device and shows no shift or beam steering effect. This can be explained as the negligible thickness of the coating compared to the length of the cavity.

### 3 Coating design and results

Although the AR coating with near 0 % reflectivity achieved significant improvements in output performance under pulsed operation. Nevertheless, for LWIR QCLs, it is necessary to optimize the reflectivity for ensuring further improvement of  $P_{max}$  and WPE under CW operation. The slope efficiency  $\eta_s$  of LWIR QCLs is defined as<sup>[23]</sup>

$$\eta_s = \frac{N}{1 + 1/\beta} \eta_i \left( \frac{\alpha_m}{\alpha_m + \alpha_w} \right), \quad (2)$$

$$\beta = \frac{1 - R_{front}}{1 - R_{back}} \sqrt{\frac{R_{back}}{R_{front}}}$$

where  $\beta$  takes into account the unequal power distribution from asymmetry in facet reflectance<sup>[24]</sup>,  $N$  is the number of stages, and  $\eta_i$  is the internal quantum efficiency per stage.  $R_{back}$  and  $R_{front}$  are the reflectivity of the back and front facets. According to Eq. (1) and (2), we can derive the internal parameters of the laser through the changes in  $J_{th}$  and  $\eta_s$  of devices with different coating states (different  $\alpha_m$ ) under pulsed operation, as follow:  $J_{tr} = 1.43 \text{ kA/cm}^2$ ,  $\alpha_w = 2.1 \text{ cm}^{-1}$ ,  $g\Gamma = 8.8 \text{ cm/kA}$ <sup>[10]</sup>. By introducing additional resonant waveguide loss  $\alpha_{w, res} =$

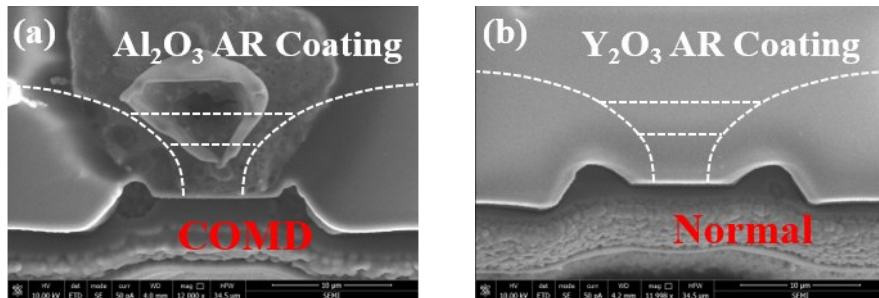


Fig.4 SEM image of the front facet of the laser coated with (a)  $\text{Al}_2\text{O}_3$  and (b)  $\text{Y}_2\text{O}_3$  AR coating after testing  
图4 镀(a) $\text{Al}_2\text{O}_3$ 和(b) $\text{Y}_2\text{O}_3$  AR膜的激光器在测试后的前腔面扫描电镜图

$g\Gamma J_{tr}=12.6 \text{ cm}^{-1}$ , the total waveguide loss is obtained as  $\alpha_w + \alpha_{w, \text{res}}=14.7 \text{ cm}^{-1}$ [25].

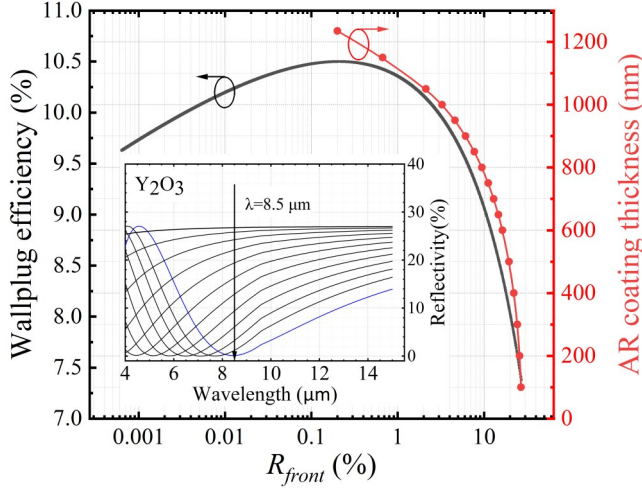


Fig. 5 Predicted  $WPE$  and AR coating thickness as a function of front facet AR reflectivity. Inset: the reflectance curves for different  $\text{Y}_2\text{O}_3$  AR coating thicknesses.

图5 预测的WPE和AR膜厚度与前腔面AR膜反射率函数关系,插图:不同 $\text{Y}_2\text{O}_3$  AR膜厚度的反射率曲线

In the simple Rigrod analysis, i. e. [26], assuming uniform gain saturation, the device  $WPE$   $\eta_w$  at the roll-over current density  $J_{max}$  can be expressed as [10]

$$\eta_w = \frac{Nh\nu}{eV_{max}} \left( 1 - \frac{J_{th}}{J_{max}} \right) \eta_i \frac{\alpha_m}{\alpha_w + \alpha_m}, \quad (3)$$

where  $h\nu$  is the photon energy,  $V_{max}$  is the voltage at  $J_{max}$ . Therefore, for LWIR QCLs, the back cavity is generally a metallic HR coating, and the appropriate  $R_{front}$  is selected by adjusting the front cavity AR coating to achieve both high  $\eta_s$  and high  $WPE$ . Figure 5 shows the relative  $WPE$  and AR coating thickness as a function of  $R_{front}$  predicted by Eq. (3) using the above internal parameters. The inset shows the reflectance curves for different  $\text{Y}_2\text{O}_3$  AR coating thicknesses, where  $R_{front}$  increases from 0.2 to 27 % by reducing the coating thickness, starting from

a quarter-wave thickness. The measured  $WPE$  is approximately 18 % lower than the model predictions due to reduced slope efficiency between threshold and roll-over [10]. Although pulsed  $WPE$  coincidentally is maximum at  $R_{front}=0.2 \%$  and then decreases with increasing front cavity reflectivity,  $R_{front}=0.2 \%$  is not conducive to power extraction for CW operation. Therefore, in order to ensure a high  $WPE$  and prevent the additional self-heating effect caused by the increase in  $J_{th}$ , the 3 mm cavity length device was chosen with the same  $\alpha_m=4.4 \text{ cm}^{-1}$  as the uncoated device. Finally, an 850 nm single-layer  $\text{Y}_2\text{O}_3$  AR coating with a reflectivity of about 7.5 % was applied by adjusting the AR coating thickness.

The  $L$ - $I$ - $V$  and  $WPE$  curves of the HR-AR ( $R \approx 7.5 \%$ ) coated device under 298 K pulsed and CW operation are shown in Figure 6 (a) and (b) respectively. The threshold current density under pulsed operation is  $J_{th}=1.79 \text{ kA/cm}^2$ , along with  $\eta_s = 1.15 \text{ W/A}$ ,  $WPE=7.20 \%$  and  $P_{max}=1.65 \text{ W}$ , and the threshold current density under CW operation is  $J_{th}=2.71 \text{ kA/cm}^2$ , along with  $\eta_s = 0.93 \text{ W/A}$ ,  $WPE=4.18 \%$  and  $P_{max}=0.73 \text{ W}$ . After optimization of AR coating reflectivity, compared to uncoated device, the HR-AR device showed 80 % and 88 % improvements in  $WPE$  and  $P_{max}$  under pulsed operation, respectively, while significant improvements of 106 % and 91 % were also obtained under CW operation. A more suitable reflectivity may exist at  $R_{front}=0.2$  to 7.5 %, allowing the power extraction under CW operation to be further increased. Furthermore, utilizing a device of the same size as in Ref. [18] along with  $\text{Y}_2\text{O}_3$  coatings with optimized reflectivity, the output performance will be significantly improved.

## 4 Conclusions

In summary, we compared the application of  $\text{Al}_2\text{O}_3$  and  $\text{Y}_2\text{O}_3$  coatings in LWIR QCLs without beam steering effect, and proved that  $\text{Y}_2\text{O}_3$  is more suitable for power extraction of high-performance LWIR QCLs compared to  $\text{Al}_2\text{O}_3$ . The LWIR QCL with  $\lambda \sim 8.5 \mu\text{m}$  was applied with a  $\text{Y}_2\text{O}_3$  coating with a reflectivity close to 0 %, which is suitable for power extraction under pulsed operation and

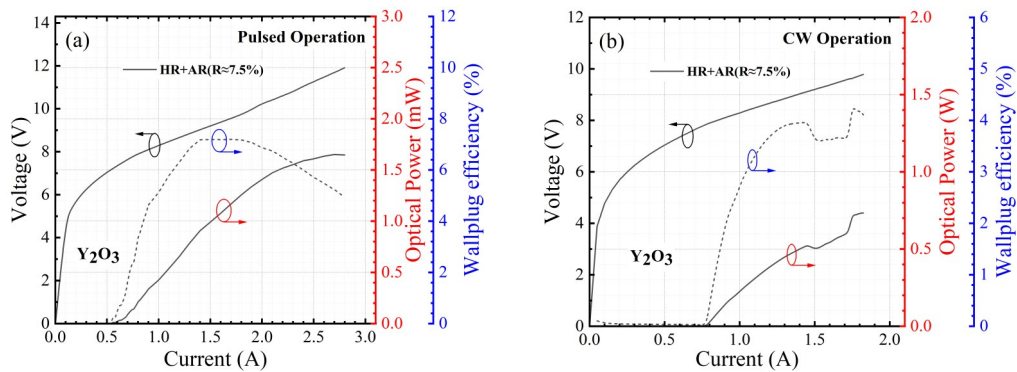


Fig. 6  $L$ - $I$ - $V$  and  $WPE$  curves of the QCL with optimized front facet  $\text{Y}_2\text{O}_3$  AR coating reflectivity under (a) pulsed and (b) CW operation at 298K

图6 具有优化前腔面 $\text{Y}_2\text{O}_3$  AR膜反射率的LWIR QCL在298K时(a)脉冲和(b)连续操作下的 $L$ - $I$ - $V$ 和 $WPE$ 曲线

obtained a peak power of 2.19 W and WPE of 8.8 %. Considering self-heating effects,  $\text{Y}_2\text{O}_3$  AR coated device with a reflectivity of 7.5 % showed a maximum pulsed peak power of 1.65 W and CW output power of 0.73 W at 298 K, which were 88 % and 91 % higher than uncoated lasers, respectively. In the future, by improving the epitaxial performance and combining the power extraction of  $\text{Y}_2\text{O}_3$  AR coating, higher performance LWIR QCLs will be obtained.

## References

- [1] SHARMA R C, KUMAR S, KUMAR S, *et al.* Photoacoustic remote sensing of suspicious objects for defence and forensic applications [J]. *Spectrochimica Acta Part A: Molecular and Biomolecular Spectroscopy*, 2020, **224**: 117445.
- [2] SUN Y Q, YANG K, LIU J H, *et al.* High sensitivity and fast detection system for sensing of explosives and hazardous materials [J]. *Sensors and Actuators B-Chemical*, 2022, **360**: 131640.
- [3] SPITZ O, DIDIER P, DURUPT L, *et al.* Free-space communication with directly modulated mid-Infrared quantum cascade devices [J]. *IEEE Journal of Selected Topics in Quantum Electronics*, 2022, **28** (1): 1–9.
- [4] Patel C K N, LYAKH A, MAULINI R, *et al.* QCL as a game changer in MWIR and LWIR military and homeland security applications [C]. *Micro-and Nanotechnology Sensors, Systems, and Applications IV*. SPIE, 2012, **8373**: 599–607.
- [5] ZHOU W, LU Q Y, WU D H, *et al.* High-power, continuous-wave, phase-locked quantum cascade laser arrays emitting at 8  $\mu\text{m}$  [J]. *Opt Express*, 2019, **27**(11): 15776–15785.
- [6] SCHUNDLER E C, MANSUR D J, HILTON M, *et al.* Multipath extinction detector for chemical sensing [C]. *Chemical, Biological, Radiological, Nuclear, and Explosives (CBRNE) Sensing XXIII*. SPIE, 2022, **12116**: 208–217.
- [7] JOHARIFAR M, DELY H, PANG X D, *et al.* High-speed 9.6- $\mu\text{m}$  long-wave infrared free-space transmission with a directly-modulated QCL and a fully-passive QCD [J]. *Journal of Lightwave Technology*, 2023, **41**(4): 1087–1094.
- [8] TROCCOLI M, LYAKH A, FAN J Y, *et al.* Long-wave IR quantum cascade lasers for emission in the  $\lambda = 8\text{--}12\ \mu\text{m}$  spectral region [J]. *Optical Materials Express*, 2013, **3**(9): 1546–1560.
- [9] XIE F, CANEAU C, LEBLANC H P, *et al.* Watt-level room temperature continuous-wave operation of quantum cascade lasers with  $\lambda > 10\ \mu\text{m}$  [J]. *IEEE Journal of Selected Topics in Quantum Electronics*, 2013, **19**(4): 1200407–1200407.
- [10] MAULINI R, LYAKH A, TSEKOUN A, *et al.* High power thermoelectrically cooled and uncooled quantum cascade lasers with optimized reflectivity facet coatings [J]. *Applied Physics Letters*, 2009, **95**(15).
- [11] ZHOU W J, WU D H, LU Q Y, *et al.* Single-mode, high-power, mid-infrared, quantum cascade laser phased arrays [J]. *Scientific Reports*, 2018, **8**: 14866.
- [12] NGUYEN J, YU J S, EVANS A, *et al.* Optical coatings by ion-beam sputtering deposition for long-wave infrared quantum cascade lasers [J]. *Applied Physics Letters*, 2006, **89**(11).
- [13] WANG F, SLIVKEN S, RAZEGHI M. High-brightness LWIR quantum cascade lasers [J]. *Optics Letters*, 2021, **46**(20): 5193–5196.
- [14] HERZOG W D, GOLDBERG B B, UNLU M S. Beam steering in narrow-stripe high-power 980-nm laser diodes [J]. *IEEE Photonics Technology Letters*, 2000, **12**(12): 1604–1606.
- [15] PAGE H, COLLOT P, DE ROSSI A, *et al.* High reflectivity metallic mirror coatings for mid-infrared ( $\lambda \approx 9\ \mu\text{m}$ ) unipolar semiconductor lasers [J]. *Semiconductor Science and Technology*, 2002, **17**(12): 1312.
- [16] NIU S Z, LIU J Q, ZHAO Y, *et al.* High-performance bound-to-continuum quantum cascade lasers at  $\lambda \sim 8\ \mu\text{m}$  [J]. *Journal of Nanoscience and Nanotechnology*, 2018, **18**(11): 7498–7501.
- [17] SUN Y Q, YIN R, ZHANG J C, *et al.* High-performance quantum cascade lasers at  $\lambda \sim 9\ \mu\text{m}$  grown by MOCVD [J]. *Optics Express*, 2022, **30**(21): 37272–37280.
- [18] FEI T, ZHAI S, ZHANG J, *et al.* High power  $\lambda \sim 8.5\ \mu\text{m}$  quantum cascade laser grown by MOCVD operating continuous-wave up to 408 K [J]. *Journal of Semiconductors*, 2021, **42**(11): 112301.
- [19] KISCHKAT J, PETERS S, GRUSKA B, *et al.* Mid-infrared optical properties of thin films of aluminum oxide, titanium dioxide, silicon dioxide, aluminum nitride, and silicon nitride [J]. *Applied Optics*, 2012, **51**(28): 6789–6798.
- [20] NIGARA Y. Measurement of the optical constants of yttrium oxide [J]. *Japanese Journal of Applied Physics*, 1968, **7**(4): 404.
- [21] TROPF W J, THOMAS M E. Yttrium oxide ( $\text{Y}_2\text{O}_3$ ) [M]. *Handbook of Optical Constants of Solids*. Academic Press, 1997: 1079–1096.
- [22] SLIVKEN S, EVANS A, YU J S, *et al.* High power, continuous-wave, quantum cascade lasers for MWIR and LWIR applications [C]. *Quantum Sensing and Nanophotonic Devices III*. SPIE, 2006, **6127**: 15–24.
- [23] YU J S, SLIVKEN S, EVANS A J, *et al.* High-performance continuous-wave operation of  $\lambda \sim 4.6\ \mu\text{m}$  quantum-cascade lasers above room temperature [J]. *IEEE Journal of Quantum Electronics*, 2008, **44**(8): 747–754.
- [24] VANDERZIEL J P, LOGAN R A, DUPUIS R D. High-power (Al-Ga) As strip-buried heterostructure lasers [J]. *IEEE Journal of Quantum Electronics*, 1985, **21**(10): 1659–1665.
- [25] WITTMANN A, HUGI A, GINI E, *et al.* Heterogeneous high-performance quantum-cascade laser sources for broad-band tuning [J]. *IEEE Journal of Quantum Electronics*, 2008, **44**(11): 1083–1088.
- [26] RIGROD W W. Homogeneously broadened CW lasers with uniform distributed loss [J]. *IEEE Journal of Quantum Electronics*, 1978, **14** (5): 377–381.